International Journal of Engineering Trends and Technology
ISSN: 2231 – 5381 / https://doi.org/10.14445/22315381/IJETT-V70I12P216

Volume 70 Issue 12, 147-159, December 2022

Original article

An Effective Diagnosis of Diabetic Retinopathy Based on 3d Hybrid Squeezenet Architecture

B. Venkaiahppalaswamy[1], PVGD Prasad Reddy[2], Suresh Batha[3]

[1,2]*Department of Computer Science and Systems Engineering, Andhra University Visakhapatnam, Andhra Pradesh,, India*
[3]*Additional Director at Software technology, Parks of India, Gujarat, India*

[1]*Corresponding Author : bvaswamy123@gmail.com*

Received: 19 August 2022 Revised: 13 November 2022 Accepted: 24 November 2022 Published: 24 December 2022

Abstract *- Diabetic retinopathy (DR), which affects an increasing number of people of all ages who have the disease, causes vision issues. Computer-aided diagnosis technology, particularly for the development of deep learning techniques, has become widely used in research for the screening of DR. Accurate annotation is more expensive than other vision tasks since most deep learning-based DR grading models need many annotations to provide data direction, and it is difficult for professionals to detect tiny lesion locations from fundus images. This paper developed a deep learning-based 3D hybrid squeezenet architecture for multiclass DR classification. Here, 3D CNN and squeeznet are hybridized to detect the classes such as mild, moderate proliferate accurately, and severe DR. In addition, an effective data augmentation/ enhancement is achieved using Gaussian blurring and random shift, as well as their combination. The proposed system for data augmentation in the initial stage is to lessen the overfitting issue in 3D hybrid squeeznet to acquire a more trustworthy and robust classification. In this case, intend to categorize several classes, and constructing a 3-D based hybrid network is a superior design since it will train the data more effectively and with less complexity. Finally, a performance study with and without data augmentation is performed to assess the efficiency of the proposed design. The experimental results of the proposed methodology attain enhanced performance than the different compared techniques in terms of accuracy, precision, recall, F1 score, sensitivity, specificity, kappa score and run time.*

Keywords *- Diabetic retinopathy, Deep learning, Gaussian blurring, Random shifting, Data augmentation.*

1. Introduction

Diabetes is a chronic metabolic condition that causes the patient's blood glucose levels to increase alarmingly over an extended period. Diabetes can cause serious, life-threatening consequences and early death [1]. Most diabetics fall into the 40 to 59 age range, where one in two of the world's 7.79 million inhabitants are unaware of the effects of diabetes, and they are uninformed about their condition [2]. However, Type 2 diabetic cases are now being documented in people of various ages, including children, teenagers, and the elderly [3]. Diabetes has many harmful effects on human health [4]. The most frequent side effects of chronic high blood sugar levels are DR, lower limb amputation, kidney failure, cardiovascular disease, and early mortality.

DR is a condition that damages the internal vessels which carry blood in the retina. Generally speaking, DR progresses through two stages: proliferative DR (PDR) and non-proliferative DR (NPDR). In NPDR, blood vessel (BV) leaks in the eyes, causing an accumulation of glucose that causes the retina to swell, known as macular edema [5]. If the swelling is severe enough, the BVs may become stopped, which would cause macular ischemia. In each case, the patient experiences partial, total, or occasionally intermittent vision loss. In PDR, new BVs begin to form in the retina. This condition is termed neovascularisation, which happens in the later phase of diabetes. The new BVs are incredibly delicate and narrow, making them more prone to bleeding. This hemorrhage's blood causes partial or total eyesight loss [6- 7]. People with type 1 diabetes had more excellent rates of PDR and other types of DR than people with type 2 diabetes [8]. In individuals aged 20 to 74, DR is the predominant reason for vision loss and preventable blindness, especially in middle-income and high-income nations [9]. Only a patient with diabetes for at least ten years without proper eye examination, diagnosis, or treatment can develop DR. Everyone with diabetes is susceptible to DR [10]. About one in three people with diabetes is reported to have some degree of DR. By doing health examinations and treating diabetes systematically, DR can always be avoided if it is identified early enough [11].

Optical coherence tomography (OCT) and Fluorescein angiography (FA) are two commonly used diagnostic procedures for DR. When using OCT, procedures are carried out to get cross-sectional images of the retina, so it becomes easier to spot problems relating to fluid leakages or retinal tissue damage [12]. FA involves injecting a dye into the vein of the patient's arm and then taking photographs of the BVs in the eyes can detect the signs of blockages, leaks, and hemorrhages [13]. This traditional diagnosing method of DR is a labor-intensive and manual process that calls for an ophthalmologist or other qualified

physician to look over and assess digital color fundus images of the retina to spot lesions connected to the vascular irregularities brought on by the illness [14].

Recent studies concentrated on various DR techniques, which are accomplished with Deep Learning (DL), an Artificial Intelligence (AI) division. The most precise results in detecting hidden layers in various AI tasks, including medical image interpretation, are produced by AI models and in AI, specifically "DL" [15- 16]. Using DL models to categorize diseases facilitates medical decision-making and enhances resolute consideration [15- 16]. To diagnose DR, several methods have been suggested for the analysis of the fundus images. For instance, an upgraded version of the Inception-v4 ensembling method [33], active deep learning convolutional neural network (ADL-CNN) model [18], region-based Convolution Neural Network (RCNN) combined with Wild Geese Algorithm (WGA) [19] and Autoregressive-Henry Gas Sailfish Optimization (Ar-HGSO) [20].

1.1. Research Gap

Retinopathy research has a limited number of publicly accessible datasets. The fact that many of the employed images are blurry makes them practically useless, which interferes with the efficiency of the models by producing poor training. Deep learning models need a lot of data to train on, which is an issue. When a model's training is too closely tied to the training dataset, overfitting occurs, leading to inconsistent results when the model is tested on external data. Due to a lack of datasets, this gap exists. Much processing power, namely GPU, is needed for deep learning. The high cost of these forces researchers to look for online sources, occasionally charging for extended. Images are not in focus and have an uneven angle, which results in light diffusion in the retina. Various imaging modalities employ Artificial Intelligence (AI) in fundus images in existing works, and deep learning architectures are discussed. With certain restrictions, the literature used to inform this study mentioned higher throughput in systematically managed conditioned occurrences. The features retrieved in the classification models required proper professional understanding, resulting in a drawn-out procedure, a lack of abstraction, and the impossibility of handling larger datasets.

The main contributions of the presented methodology are described,

- The gaussian blurring and random shifting approaches enhance the model's generalization performance.
- To develop a deep learning-based 3D hybrid squeezenet architecture for multiclass DR classification. Here, 3D CNN and squeeznet are hybridized to accurately detect the classes such as mild, moderate proliferate, and severe DR.
- Different performance metrics are analyzed and compared with various existing approaches to validate the performance of DR detection.

The organization of the proposed work is summarised as follows: Section 2 provides the recent related works, section 3 describes the proposed methodology, section 4 explains the result and discussion, and section 5 provides the conclusion.

2. Related Work

Muhammad Mohsin Butt et al. [34] proposed a combined method for the identification and categorization of DR in fundus photographs of the eyes. The transfer learning (TL) technique was applied for feature extraction on pre-trained CNN models, and the extracted features were combined to produce a hybrid feature vector (HFV). Various classifiers get HFV to categorize fundus images in binary and many classes. Multiple measures were used to gauge system performance, and the results were contrasted with more contemporary methods of DR detection. The suggested technique significantly boosts fundus image DR detection performance. The proposed improved technique has the maximum accuracy for multiclass classification (89.29%) and binary classification (97.8%). Improvements can be made to the results, including data augmentation and using various preprocessing methods to eliminate noise and artefacts from the input images.

Eman AbdelMaksoud et al. [22] proposed E-DenseNet, a revolutionary hybrid deep learning approach which combined TL-based EyeNet and DenseNet models. The suggested DL-based computer-aided diagnosis (DL CAD) system, built on the E-DenseNet framework, successfully distinguished between healthy and disease-related cases using various colour fundus images. The sensitivity (SEN), average accuracy (ACC), Dice similarity coefficient (DSC), specificity (SPE), calculation time (T) in minutes (m), and quadratic Kappa score (QKS) for the proposed method were 96 percent, 91.2 percent, 92.45 percent, 69 percent, 3.5 minutes, and 0.883 respectively.

Abubakar M. Ashir et al. [23] suggested a new method that used a quantized Haralick feature that uses local extrema information to extract a feature from the fundus image. The quantized characteristics used the multi-resolution information of various symptoms in DR and encoded the textural Haralick features. Long Short-Term Memory Network (LSTMN) and local extrema pattern offered a probabilistic method for more accurate image segment analysis, which reduces the likelihood of false positive results. On two separate publicly available datasets, the suggested method examines the retinal vasculature and hard-exudate signs of DR. But, the proposed method excludes the detection of further DR symptoms, such as hemorrhage and micro aneurysm.

Lakshmana Kumar Ramasamy et al. [24] developed an automated method for classifying DR by merging the derived features from Ridgelet Transform and texture analysis methods (GLRLM and GLCM). In order to detect DR, the retrieved features from the provided method were classified using the Sequential Minimal Optimization (SMO) classifier. Results of the trials show that the proposed method was both high-quality and effective when

utilized with the publicly available retinal image datasets for performance analysis that achieved 98.87 percent sensitivity, 97.05 percent accuracy, 95.24 percent specificity on the DIARETDB1 dataset, and 90.9 percent sensitivity, 91.0 percent accuracy, 91.0 percent specificity on KAGGLE dataset. The suggested method also has some drawbacks because it uses all Ridgelet and textural data, which may contain features that were not significant for DR detection and increase calculation time and occasionally even lower recognition accuracy.

Muhammad Kashif Yaqoob et al. [25] suggested a method using Random Forest classification with the help of fine-tuned ResNet-50 feature map. Using five-category EyePACS datasets and two-category Messidor-2 datasets, the suggested method was compared against five state-of-the-art approaches. No Referable Diabetic Macular Edema Grade (DME) and Referable DME were the two categories on the Messidor-2 dataset, respectively, while PDR, Severe DR, Moderate DR, Mild DR, and No DR were the five categories. The findings demonstrated that the suggested strategy performed better than comparable approaches and attained 96% and 75.19% accuracy for these datasets. The suggested method outperforms ResNet-50, Inception-v3, VGG-19, VGG16, and MobileNet, six current state-of-the-art designs. This suggested approach cannot operate on unfiltered images in real time. So more testing in real-world circumstances was essential for clinical applications, and the system should be strengthened.

S. Hemavathi and Dr. S. Padmapriya [26] proposed employing the support vector machine method to identify diabetic retinopathy automatically. An image of the retina was used as the project's input and sent to the preprocessing stage for noise removal. The method of feature extraction was applied to the preprocessed image. HOG and SURF features from the provided image will be extracted as part of the feature extraction process. The SVM classifier was provided with the retrieved picture. Whether diabetic retinopathy was present in the image or not will be determined by the classifier.

Dr. Shubhangi and Tasleem Begum [27] provide a method for ejected material's programmed destination. Expel the non-expelled in two stages using the Gradient Vector Flow Snake computation and area growing division calculation, such as the optic plate, veins, and blood clumping. It encourages location productivity by masking fake exudates. At that point, identify exudates using a division computation based on Gabor channel surface edge detection. Only Gabor channels tuned to two superior frequencies and four directions were used to reduce the processing complexity.

S. Regina Lourdhu Suganthi et al. [28] introduced machine learning techniques that extract numerous features from the eye image utilizing domain knowledge to reveal different elements of the disease pattern. Machine learning algorithms for automatic classification are often rigid. Deep learning has been utilized for high-accuracy automatic categorization and prediction. The preprocessed eye image data set was used to train the classifier for binary classification, determining whether the patient's eye was infected or normal. The model was tested using several metrics, including Precision, Recall, and F-Score.

Manojkumar S B and H S Sheshadri [29] identified all stages of diabetic retinopathy during the early stage by developing regions of a retina image to show the specific region of interest in terms of its severity level by collecting extensive data from Kaggle, DIARETDB0, and DIARETDB1 datasets and then pre-trained the models and applied to LPB and deep learning classifiers and able to obtain results and analyze those hypothesis results and achieve 65% predicted correctly.

3. Proposed Methodology

This paper developed a deep learning-based 3D hybrid squeezenet architecture for multiclass Diabetic Retinopathy (DR) classification. Here, 3D CNN and squeeznet are hybridized to detect the classes such as mild, moderate proliferate accurately, and severe DR. In addition, an effective data augmentation/ enhancement is achieved using Gaussian blurring and random shift, as well as their combination. Here, a system for data augmentation was proposed in the initial stage to lessen the overfitting issue in 3D hybrid squeeznet to acquire a more trustworthy and robust classification.

In this case, intend to categorize several classes, and constructing a 3-D-based hybrid network will be a superior design since it will train the data more effectively and with less complexity. Finally, a performance study with and without data augmentation is performed to assess the efficiency of the proposed design. The architecture of 3D hybrid squeeznet-based DR classification is depicted in figure 1.

3.1. Pre-Processing using Data Augmentation

Examining unlabelled retinal images is the most significant task in DR grading work. The main issue with DR classification is the lack of a sufficient train sample in real-time circumstances. Adding augmentation in deep learning is a common and simple method for producing changes for unlabelled raw fundus images that contain consistent identification information but are close to realistic circumstances. In order to solve this issue and enhance the generalization performance of the model, gaussian blurring and random shifting is performed in the data.

Gaussian blurring is the technique used to blur a picture using a gauss function. In particular, the random shift is a helpful augmentation since it modifies the angles at which objects appear in the training dataset. Here proposed a system for data augmentation in the initial stage to lessen the overfitting issue in 3D hybrid squeeznet to acquire a more trustworthy and robust classification.

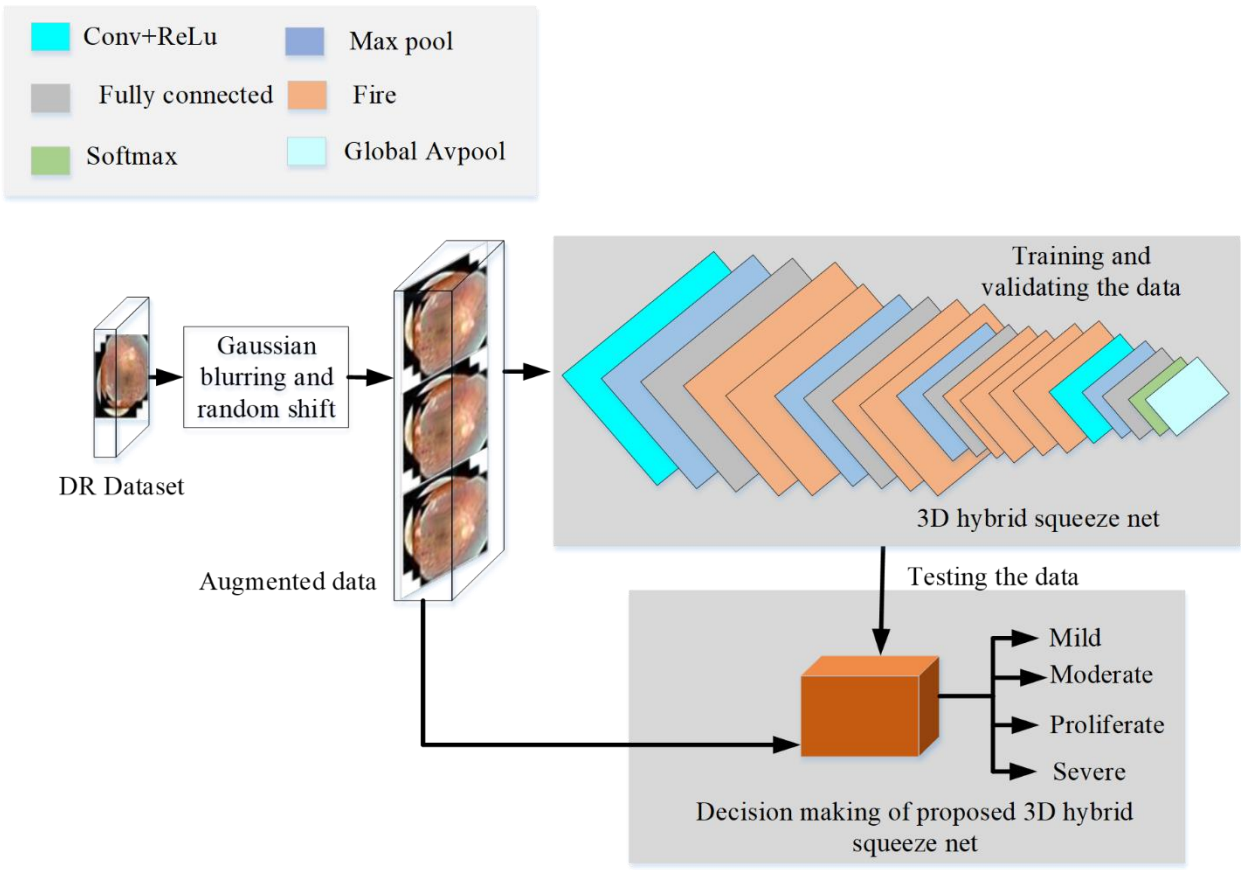

Fig. 1 Architecture of proposed 3D hybrid squeeznet-based DR classification

3.1.1. Gaussian Blurring and Random Shifting

The primary concept behind this technique is to update a pixel's value by taking the average of its surrounding pixels. Here compute a weighted average rather than the average of all neighbouring pixels.

$$G(a,b) = \frac{1}{2\pi\sigma^2} e^{-(a^2+b^2/2\sigma)^2}, \quad (1)$$

Where a and b are the coordinates of pixels in the Gaussian blur kernel, $\sigma$is the standard deviation. The Gaussian blurred image (I_B) acquired by,

$$I_B = I \oplus G(a,b) \quad (2)$$

The convolutional operator is denoted as$\oplus$.

The effect of Gaussian blur relies on the size of the Gaussian blur kernel and the standard deviationσ. The average weight of each pixel has the maximum value when this value converges on a corresponding blur pixel. These filters operate by swiping an $n \times n$ matrix across an image with either a Gaussian blur filter, which produces a blurrier image or a high contrast vertical or horizontal edge filter, which produces a sharper image along edges. It makes sense that blurring images for Data Augmentation could result in greater resilience to motion blur during testing.

It should be noted that in order to avoid cropping edges, an image must either have its top and bottom corners removed or be more extensive than usual random shifting is employed. The corners of the image are undefined after rotation and must be padded. A domain set is required when the images of the objects do not rotate spontaneously. The bounding box must rotate with the image, and rotation causes the bounding box to enlarge.

To examine the effects of these techniques on both classification tasks, here used random weak Gaussian blurring and random shift as data augmentation/enhancement techniques, as well as their combination.

3.2. DR Classification using 3D Hybrid Squeeznet

SqueezeNet is a lightweight structure with fewer structural parameters and fewer calculations, and its structure and classification accuracy meet the application requirements. SqueezeNet uses only 1×1 and 3×3convolution kernels, and its goal is to achieve the best classification accuracy and to reduce network complexity. The proposed approach for data augmentation in the early stage is to reduce overfitting in 3D hybrid squeezeNet to provide a more reliable and robust classification. In this situation, a 3-D-based hybrid network is a better design because it trains the data more effectively and with less complexity.

The developed deep learning-based 3D hybrid squeezenet architecture is used for multiclass DR classification. Here, 3D CNN and squeeznet are hybridized to detect the classes such as mild, moderate proliferate accurately, and severe DR. The architecture of the 3D hybrid squeezenet is shown in figure 2.

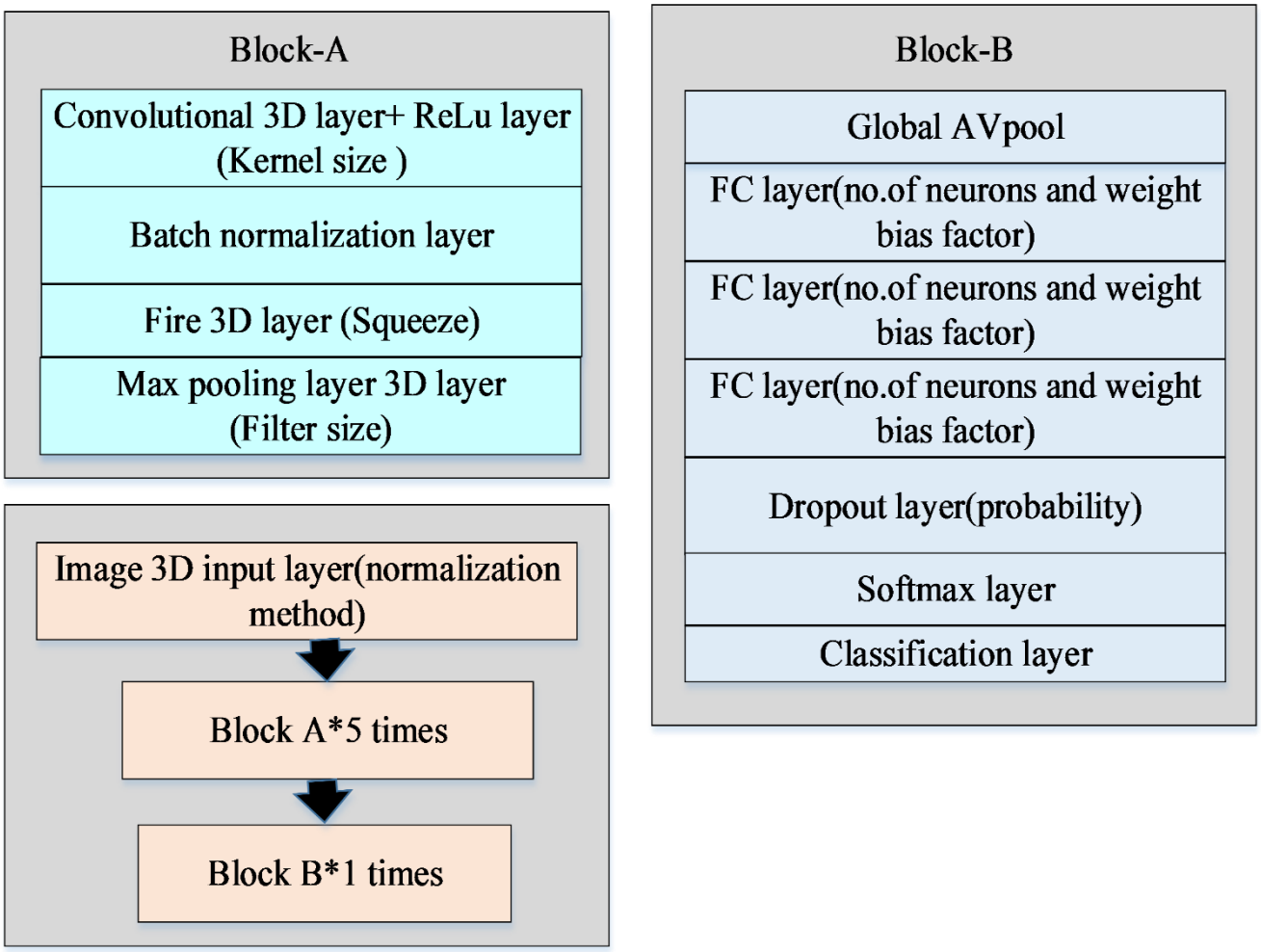

Fig. 2 Architecture of 3D hybrid squeeznet

3.2.1. Convolutional Layer

Each feature map in the convolutional layer contains a set of neurons, and feature maps are also referred to as depth slices. Equation (3) describes the convolutional operation's output in a convolutional layer. The size of the kernel filter is denoted by$f$, the feature mappings are represented by$M$, the bias is denoted as$b$, and the weight of the kernel is denoted byw_j. The symbol represents a convolutional layer's outputY_i^1, where i represents the layer's ith feature map.

$$Y_i^1 = b_i^1 + \sum_{j=1}^{M_1(i-1)} f_{i,j^1} \times w_j^{(i-1)} \quad (3)$$

3.2.2. Rectified Linear Unit (Relu) Activation Layer

The output of a neuron in 3D-CNN is determined by a nonlinear activation function, despite the fact that the connections between neurons in 3D-CNN are of the local connection type, similar to ANN. ReLu activation function, shown in figure 2, is favoured by logistic sigmoid and hyperbolic tangent functions due to its excellent performance, quick learning curve, and simple structure. Equations (4) show the ReLu function's formula and derivative in equation (5). The gradient of the ReLu function is 0 if$Z \leq o$; otherwise, it is 1.

$$F(Z) = max(0, x) \quad (4)$$

$$F'(Z) = \begin{cases} 1 if Z > 0 \\ 0 if Z \leq 0 \end{cases} \quad (5)$$

3.2.3. Max Pooling Layer

The pooling layer is typically employed between convolutional layers to reduce the number of parameters and network calculations. As a result, the input size is reduced in all depth sections through the subsampling operation, which minimizes overfitting through network training. The pooling method reduces the input's spatial size, which leaves the depth dimension unchanged.

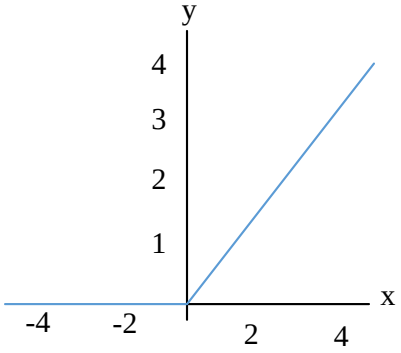

Fig. 3 Activation function of ReLu

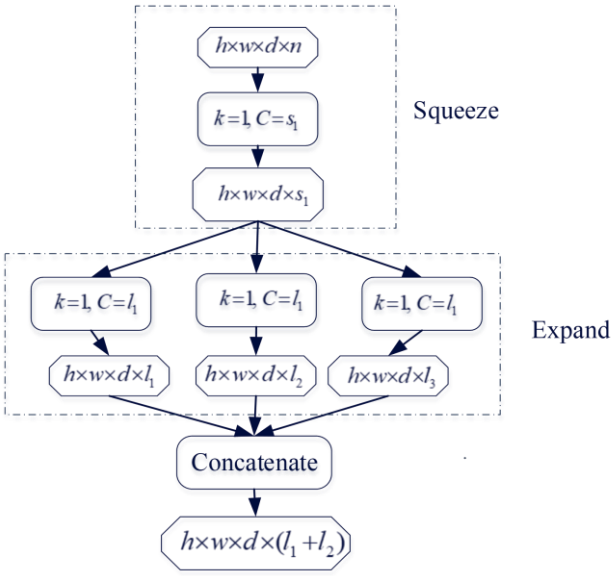

Fig. 4 Fire module operation process

$$w_2 = (\frac{w_1+f}{s}) + 1 \quad (6)$$

$$h_2 = (\frac{h_1+f}{s}) + 1 \quad (7)$$

In the pooling layer, the height and the width are obtained using equations (6) and (7). The depth, width and height in the equations are denoted as $d_1, w_1 and h_1$correspondingly, f is the kernel size, and s is the stride size.

3.2.4. Fire 3D Layer

In order to create a Fire module with a squeeze layer and an expand layer, Squeeze Net draws inspiration from the Inception module. Figure 4 depicts the Fire module's operation process. The squeeze layer compressed the input items using a $1 \times 1 \times 1$ convolution kernel to decrease the number of channels for the input elements. For multi-scale learning and concatenating, the expansion layer utilized $1 \times 1 \times 1$ and $3 \times 3 \times 3$ convolution kernels.

The input feature maps have a size of$h \times w \times d \times n$. The input feature maps first go through a squeeze layer to create output feature maps that are in $h \times w \times d \times s_1$size. The channels shrink from n tos_1, while the size of the feature maps remains constant. The squeeze layer's output feature maps are delivered into the expand layer's $1 \times 1 \times 1$ and $3 \times 3 \times 3$ convolution kernels, correspondingly. After that, concatenate the outcome of the convolution.

Only the number of channels is changed at this point to$l_1 + l_2 + l_3$. The boundary zero filling operation with 1 pixel is carried out for the input of the $3 \times 3 \times 3$ filters in the extension module in order to enable the output activation of $1 \times 1 \times 1$ and $3 \times 3 \times 3$ filters to have the same height, depth, and width. The squeeze layer and an expansion layer are activated using ReLU. In the meantime, Squeeze Net lacks a full-connection layer.

The expansion operation increases the depth while maintaining the same feature size, while the squeeze operation reduces the depth. Finally, using the concatenate operation, expansion outputs are stacked in the depth dimension of the input tensor. The squeeze operation with the kernel$W$'s output layer $F\{y\}$ can be written as,

$$F\{y\} = \sum_{Fm1=1}^{fm} \sum_{C=1}^{c} W_C^F Fm1 \quad (8)$$

In this case, $W \in \Re^{C\times1\times fm2}andF\{y\} \in \Re^n$. The feature maps of the various tensors are combined in a weighted manner to create the squeeze outputs. In the network, the global average pool turns the feature maps of the classes into one value, and the max pool layers downsample along the spatial dimensions. The softmax activation function provides the multiclass probability distributions at the network's conclusion. Thus the proposed methodology effectively classifies the DR into mild, moderate, no, proliferate, and severe DR categories.

4. Results and Discussion

The presented diabetic retinopathy classification using 3D hybrid squeeze net architecture is implemented in the python platform. The TeleOphta database is used for fundus images with exudates and microaneurysm lesions. The performance of the presented technique is examined with the existing VGG, MSANet, Inception V3, ResNet 50, and MobileNet in terms of accuracy, sensitivity, specificity, Precision, Recall, F1 measure, Kappa score, and Run time. The presented framework classifies the input into mild, moderate, no, proliferate, and severe DR categories.

4.1. Dataset Description

The dataset used to analyze the presented technique is the TeleOphta dataset. Here, 99 3D volumes were created of healthy patients using this database and 83 3D volumes of diseased subjects with evidence of exudates and microaneurysms. These volumes are divided at the subject level. Random shifting and weak Gaussian blurring augmentation techniques are used to improve the dataset.

4.2. Performance Metrics

In this section, effective performance measures like Accuracy, Sensitivity, specificity, F1-score, Precision, Recall, Kappa score, and Run time are evaluated for the performance of the presented technique.

4.2.1. Accuracy

Accuracy is determined by dividing the number of components TP and TN by the sum of the components TP, TN, FP, and FN. The following equation can be used to determine accuracy.

$$\text{Accuracy} = \frac{T_P+T_N}{T_P+T_N+F_P+F_N} \quad (9)$$

Here, T_P signifies the true positive, T_N signifies the true negative, F_P denotes the false positive and $F_N$denotes the false negative value.

4.2.2. Sensitivity

This is the overall amount of original positive data that is correctly classified.

$$\text{Sensitivity} = \frac{T_P}{T_P + F_N} \quad (10)$$

4.2.3. Specificity

The ratio of TN to the total number of components that belong to the negative class (i.e., the total of TN and FP) can be used to express it. Equation (11) displays the mathematical expression.

$$\text{Specificity} = \frac{T_N}{T_N + F_P} \quad (11)$$

4.2.4. Precision

Represented as a ratio of the total number of TP to the total number of component tags, according to the positive class (i.e., the sum of TP and FP). The precision is indicated by the term Positive Predictive Value (PPV). The following are ways to gauge precision:

$$\text{Precision} = \frac{T_P}{T_P + F_P} \quad (12)$$

4.2.5. Recall

Represented as a ratio of the total number of TP to the total number of component tags, according to the negative class (i.e., the sum of TP and FN).

$$\text{Recall} = \frac{T_P}{T_P + F_N} \quad (13)$$

4.2.6. F1- Score

It is measured using the harmonic mean of recall and precision, as shown in equation (14).

$$\text{F1-score} = \frac{2 \times Precision \times Recall}{Precision + Recall} \quad (14)$$

4.2.7. Kappa Score

Kappa can have a value between 0 and 1. Scores of 0 and 1 indicate varying degrees of agreement between raters, whereas scores of 0 and 1 indicate total agreement. A number that is lower than 0 indicates that there is less agreement than would be expected.

$$\text{Kappa score} = 1 - \frac{\sum_{i,j} W_{i,j} o_{i,j}}{\sum_{i,j} W_{i,j} E_{i,j}} \quad (15)$$

Here, o is the confusion matrix, E displays the expected rating, and W is the weight matrix derived based on the difference between the actual value and the predicted value. These three matrices are $N \times N$ in size.

4.2.8. Run Time

It is the time taken to execute the proposed methodology. For better performance, the run time should be minimum.

$$R_{time} = C_{time} - B_{time} \quad (16)$$

Here, R_{time} denotes the run time, C_{time} denotes the completion of the process and B_{time} denotes the beginning time of the process.

4.2.9. Receiver Operating Curve (ROC)

A probability graph that displays the effectiveness of a classification model at various threshold levels is called a ROC curve or Receiver Operating Characteristic curve. The curve is drawn between these two parameters: True positive rate (T_{pr}) and false positive rate (F_{pr}).

$$T_{pr} = \frac{T_p}{T_p + F_n} \quad (17)$$

4.2.10. Area Under the Curve (AUC)

The term AUC stands for Area under the ROC Curve. AUC computes the two-dimensional area under the whole ROC curve extending from (0, 0) to (0, 1). AUC computes the binary classifier performance over various thresholds and provides an aggregate metric. The value of AUC ranges from 0 to 1. Therefore, an excellent model will have an AUC close to 1, indicating a good separability measure.

4.2.11. False Positive Rate (F_{pr})

The ratio of the number of erroneous positive predictions to all negative predictions is how the false positive rate (FPR) is calculated.

$$F_{pr} = \frac{F_p}{F_p + T_n} \quad (18)$$

4.2.12. False Negative Rate (F_{nr})

The FNR stands for the percentage of positives that result in negative test results using the test.

$$F_{nr} = \frac{F_n}{T_p + T_n} \quad (19)$$

4.2.13. Negative Predictive Value (N_{pv})

NPV stands for the chance that patients with a negative screening test actually do not have the disease.

$$N_{pv} = \frac{F_n}{F_n + T_n} \quad (20)$$

4.2.14. False Discovery Rate (F_{dr})

The FDR measures how many of the rejected hypotheses were false positives.

$$F_{dr} = \frac{F_p}{T_p + F_p} \quad (21)$$

Table 1. Performance analysis of different existing techniques

Technique	Accuracy	Specificity	Sensitivity	F1 score
VGG	0.969	0.971	0.974	0.971
MSA-Net	0.981	0.982	0.983	0.982
Inception V3	0.965	0.969	0.972	0.968
ResNet 50	0.958	0.962	0.968	0.965
MobileNet	0.963	0.969	0.974	0.969
Proposed	**0.989**	**0.988**	**0.987**	**0.988**

4.2.15 Mathews correlation coefficient (M_{CC})

A correlation coefficient called MCC is calculated using four values described in equation (22)

$$M_{CC} = \frac{T_p \times T_n - F_p \times F_n}{\sqrt{(T_p+F_p)(T_p+F_n)(T_n+F_p)(T_n+F_n)}} \quad (22)$$

4.3. Performance Analysis

In this section, the performance of the presented approach is examined with the existing techniques. The comparison analysis of the presented methodology in terms of accuracy, specificity, sensitivity and F1 score is specified in table 1.

Table 1 compares the proposed technique's performance analysis with the existing VGG, multi-scale attention network (MSA-Net), inception V3, ResNet, and MobileNet techniques. Here, the presented approach attains improved accuracy, specificity, sensitivity, and F1 score than the other existing approaches. The performance in terms of accuracy is represented in figure 5. In figure 5, the proposed approach attains enhanced accuracy of 0.989 % value to the previously available techniques.

The specificity analysis of the existing and proposed are depicted in figure 6. Figure 6 illustrates that the specificity performance of the presented approach of 0.988% attains significant performance than the existing approach VGG, multi-scale attention network (MSA-Net), inception V3, ResNet, and MobileNet techniques.

Moreover, the sensitivity performance is depicted in figure 7. Figure 7 illustrates that the sensitivity performance of the presented approach of 0.987% attains a significant performance than the existing approach VGG, multi-scale attention network (MSA-Net), inception V3, ResNet, and MobileNet techniques.

Moreover, the F1 score performance is depicted in figure 8. Figure 8 illustrates that the F1 score performance of the presented approach of 0.988% attains significant performance than the existing approach VGG, multi-scale attention network (MSA-Net), inception V3, ResNet, and MobileNet techniques.

Performance evaluation in terms of precision of the suggested method compared to the earlier work for DR classification is depicted in table 2. Table 2 compares the proposed technique's performance analysis with the existing multi-Sieving, ensemble approach, red lesions, and deep learning techniques. Here, the presented approach attains improved precision value. Moreover, the precision value performance is depicted in figure 9.

Table 2. The performance comparison of proposed and existing methods in terms of precision

Techniques	Precision (%)
Multi-Sieving	81.5
Ensemble approach	80.3
Red lesions	82
Deep learning	79
Proposed	**97.5**

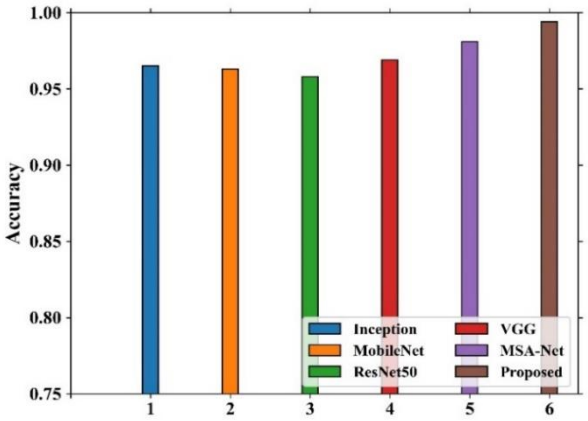

Fig. 5 Performance analysis of accuracy

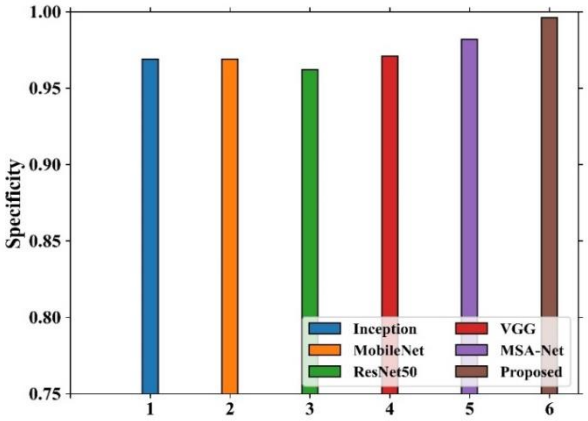

Fig. 6 Performance analysis of specificity

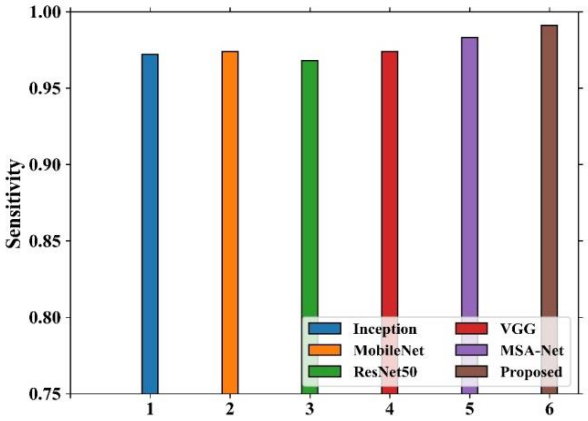

Fig. 7 Performance analysis of sensitivity

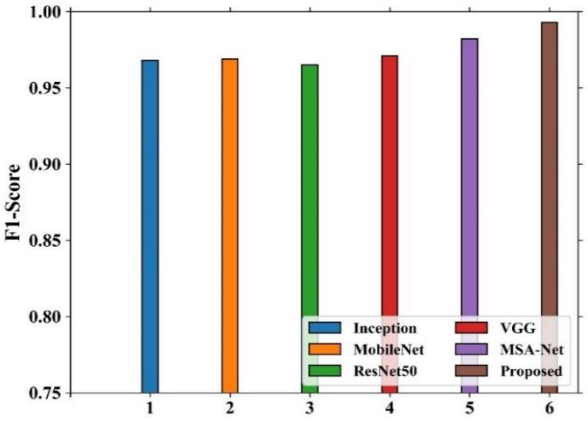

Fig. 8 Performance analysis of F1 score

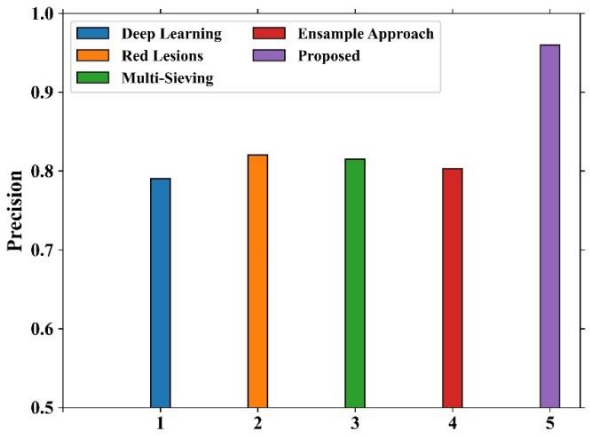

Fig. 9 Performance analysis of precision value

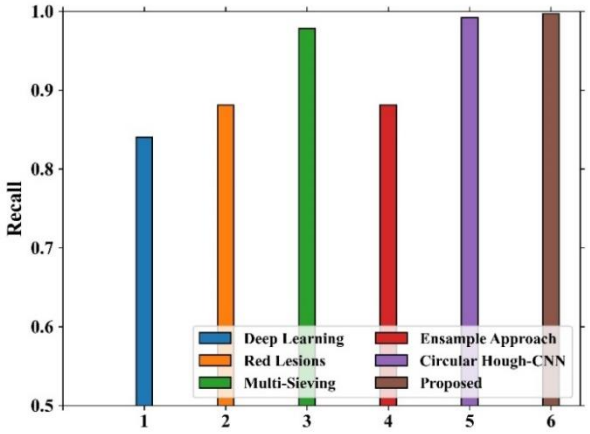

Fig. 10 Performance analysis of recall value

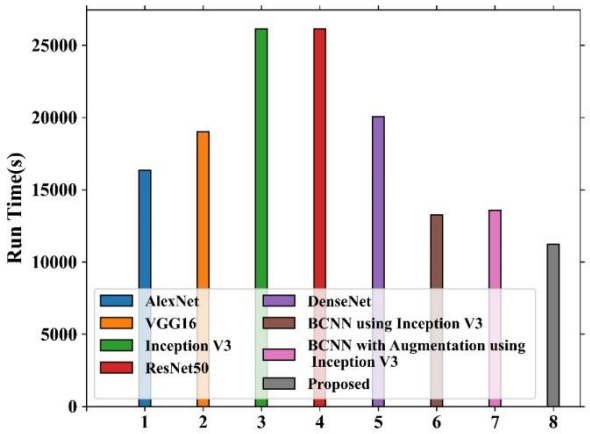

Fig. 11 Performance analysis of Run time

Table 3. The performance comparison of proposed and existing methods in terms of recall

Techniques	Recall (%)
Multi-Sieving	0.978
Ensemble approach	0.881
Circular Hough-CNN	0.992
Red lesions	0.881
Deep learning	0.84
Proposed	**99.8**

Table 4. Performance evaluation in terms of Kappa score

Technique	Kappa score
Binocular Model	0.808
MSA-Net	0.878
Inception V3	0.792
ResNet 50	0.786
MobileNet	0.770
Binocular model	0.829
Proposed	**0.932**

Figure 9 illustrates that the precision performance of the presented approach of 97.5% attains a significant performance than the existing approach, multi-Sieving, ensemble approach, red lesions, and deep learning techniques. Performance evaluation in terms of recall of the suggested method compared to the earlier work for DR classification is depicted in table 3.

Table 3 compares the proposed technique's performance analysis with the existing multi-Sieving, ensemble approach, red lesions, and deep learning techniques. Here, the presented approach attains improved recall value. Moreover, the recall performance is depicted in figure 10.

Figure 10 illustrates that the recall performance of the presented approach of 99.8% attains a significant performance than the existing approach multi-Sieving, ensemble approach, red lesions, and deep learning techniques. Performance evaluation in terms of the Kappa score of the suggested method compared to earlier work for DR classification is depicted in table 4.

The comparative findings between the suggested method and the earlier study are shown in table 3. The comparison was performed using the Kappa score. Table 3 shows that the suggested method performed better than the baseline MobileNet, ResNet, Inception V3, MSA-Net, Monocular and Binocular models. The performance improvement clarifies how well the multiclass attention mechanism works for recognizing retinopathy. The suggested 3D hybrid squeezNet method produced classification results for mild, moderate proliferate, and severe DR that was more reliable than any other method. Figure 11 depicts the run time classification between existing and proposed methods.

Figure 11 demonstrates the proposed model's runtime comparison to those of the five different models, AlexNet, VGG-16, Inception V3, Resnet 50, and DenseNet, as well as the prior BCNN model method. The run time of the proposed model only consumes 11500 seconds, which is more reliable. Figure 12 depicts the classification of data with augmentation and without augmentation.

Overall accuracy, specificity, sensitivity, precision, and F1 score have all been taken into account for the multiclass classification such as mild, moderate, proliferate, and severe DR. For each of the four tasks, such as without augmentation, with random weak Gaussian, blurred

augmentation, with randomly shifted augmentation. With mixed augmentation schemes, class-wise statistics performance measures are shown in figure 12. Combining both random weak Gaussian blurred and randomly shifted augmentation techniques is what is meant by "combined augmentations" in this context.

The model that is trained using combined augmentation methods is the one that performs the best, followed by the model that is trained using random weak Gaussian blurred augmentation method, the model that is trained using random shift augmentation scheme, and finally, the model that does not use augmentation at all performed the worst. The comparison of AUC with existing approaches is mentioned in table 5.

Table 5 represents the outcomes of AUC. The four network structures of LeNet, AlexNet, GoogleNet, and hybrid attention mechanism and residual (HAMR) [30] are compared with this experiment. The comparison experiment demonstrates that the suggested method in this research has a higher AUC than the other conventional network structures and a considerably faster rate of convergence than the other network structures.

Table 5. The comparison of AUC with existing methods

Model	AUC
AlexNet	0.7988
LeNet	0.8852
GoogleNet	0.9188
HAMR	0.9205
Proposed	**0.9901**

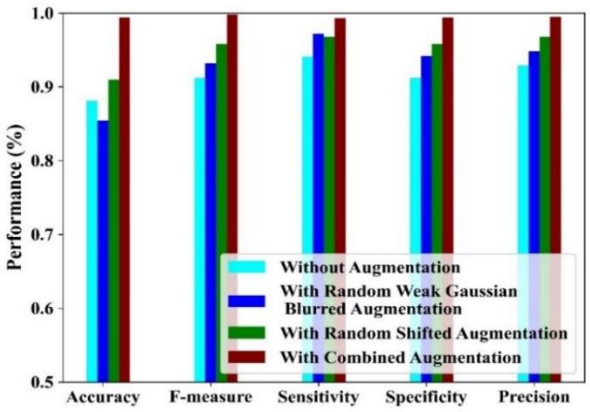

Fig. 12 Data classification with and without augmentation

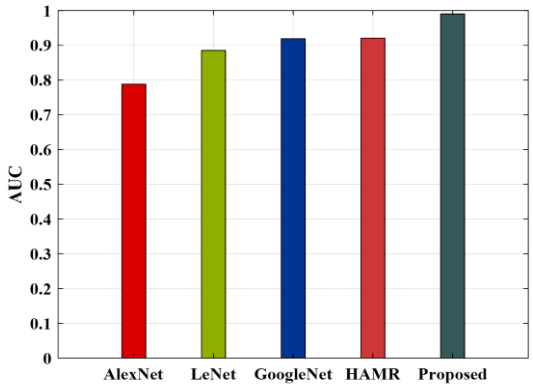

Fig. 13 The comparison of AUC with different methods

Figure 13 depicts the comparison of AUC with different methods. Comparing this experiment to LeNet, AlexNet, GoogleNet, and HAMR [30] architectures. The comparison experiment demonstrates that the proposed approach in this paper has a higher AUC than the existing architectures. AlexNet, LeNet, GoogleNet, and HAMR, the current approaches, achieve 0.7988, 0.8852, 0.9188, and 0.9205, respectively. Figure 14 shows the ROC curve plot comparison of different methods.

Figure 14 shows the ROC curve plot comparison of different methods. This experiment contrasts with the DQOR, GP, DGP, DMKDC, DLC-DR, and Inception V3 [31] approaches that are currently in use. The comparative experiment demonstrates that the proposed method in this research has a larger ROC than the other methods that are currently in use.

Table 6 shows a Performance analysis of the proposed and conventional models for detecting DR. This experiment compares many methods, including NN, KNN, SVM, GWO-DBN, WOA-DBN, MGS-ROA-DBN, and PSO-DBN [32]. The comparative experiment shows that the suggested method in this study performs better than the other available methods. The suggested method achieves very low FPR, FNR, and FDR compared to other methods. The suggested strategy achieves NPV and MCC at very high levels compared to previous methods. Figure 15 shows the performance analysis of FPR.

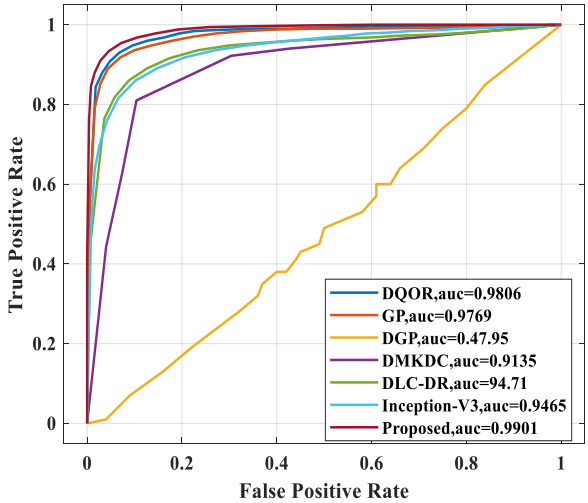

Fig. 14 ROC curve plot comparison of different methods.

Table 6. Performance analysis of the proposed and conventional models for detecting DR

Performance measures	FPR	FNR	NPV	FDR	MCC
PSO-DBN	0.12	0.36	0.87	0.36	0.51
GWO-DBN	0.07	0.22	0.92	0.22	0.69
WOA-DBN	0.10	0.31	0.89	0.31	0.57
ROA-DBN	0.06	0.18	0.93	0.18	0.75
MGS-ROA-DBN	0.04	0.13	0.95	0.13	0.81
NN	0.12	0.77	0.77	0.87	0.61
KNN	0.19	0.59	0.59	0.80	0.59
SVM	0.13	0.40	0.40	0.86	0.40
Proposed	**0.035**	**0.09**	**0.95**	**0.10**	**0.91**

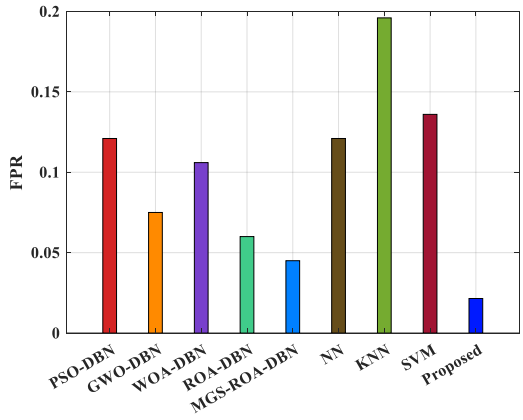

Fig. 15 Performance analysis of FPR

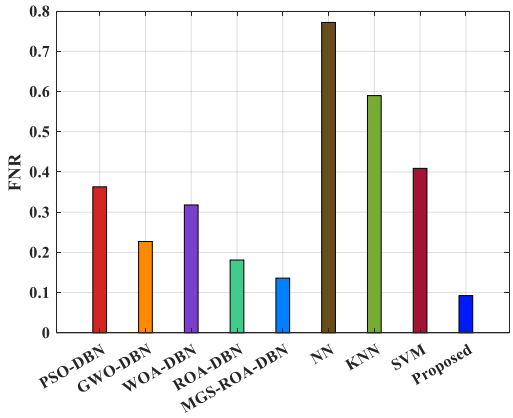

Fig. 16 Comparison of FNR with existing methods

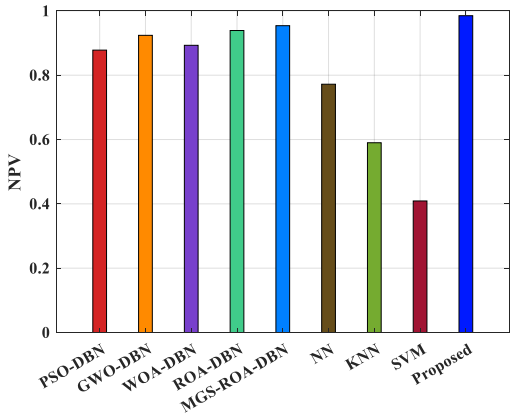

Fig. 17 Comparison of NPV with existing approaches

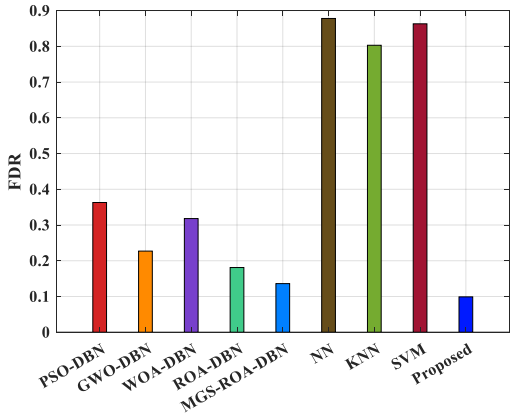

Fig. 18 Performance analysis of FDR

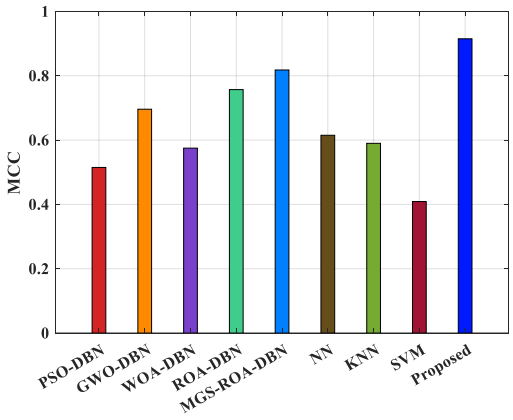

Fig. 19 Performance analysis of MCC

Figure 15 shows the performance analysis of FPR. The experiment compares the current approaches of PSO-DBN, GWO-DBN, WOA-DBN, MGS-ROA-DBN, NN, KNN, and SVM [32].

The comparative experiment shows that the researchers suggested method performs better than the others already in use. Compared to other strategies, the FPR of the suggested strategy achieves very little.

Figure 16 shows the comparison of FNR. This experiment compares many methods, including NN, KNN, SVM, GWO-DBN, WOA-DBN, MGS-ROA-DBN, and PSO-DBN [32].

The comparison shows that the suggested method performs better than the others already in use. When compared to other methods, the FNR of the suggested method is extremely low.

Figure 17 shows the comparison of NPV. The experiment compares the current approaches of PSO-DBN, GWO-DBN, WOA-DBN, MGS-ROA-DBN, NN, KNN, and SVM [32].

The comparison shows that the suggested method in this research performs better than the other currently used strategies. When compared to other methods, the NPV of the suggested strategy achieves very high levels.

Figure 18 depicts the comparison of FDR. The experiment contrasts the present methods used by NN, KNN, SVM, GWO-DBN, WOA-DBN, PSO-DBN, and MGS-ROA-DBN [32].

The comparison demonstrates that the suggested approach in this study outperforms the other approaches currently in use. The FDR of the proposed method achieves less as compared to other approaches.

The comparison shows that the suggested method from this study works better than the other methods already in use.

In comparison to previous methods, the MCC of the suggested methodology generates higher results.

5. Conclusion

This research presented an improved DR classification framework with 3D hybrid squeezNet to classify the retina image as mild, moderate, proliferate, and severe DR categories. The input image is augmented with Gaussian blurring and random shift to enhance the generalization performance of the model. Moreover, the performance of the presented technique is examined with the various existing approaches. The developed technique attained enhanced performances in terms of accuracy (98.9%), Precision (97.5%), recall (99.8%), sensitivity (98.7%), specificity (98.8%), F1 score (98.8%), Kappa score (93.2%) and Run time(11500 sec). It proves that the proposed methodology attains better outcomes than the compared approaches.

References

[1] Ashwini Tuppad, and Shantala Devi Patil, "Machine Learning for Diabetes Clinical Decision Support: A Review," *Advances in Computational Intelligence*, vol. 2, no. 2, pp. 1-24, 2022. *Crossref*, https://doi.org/10.1007/s43674-022-00034-y

[2] Thippa Reddy Gadekallu et al., "Early Detection of Diabetic Retinopathy Using PCA-Firefly Based Deep Learning Model," *Electronics*, vol. 9, no. 2, p. 274, 2020. *Crossref*, https://doi.org/10.3390/electronics9020274

[3] Shelley Spurr et al., "The Prevalence of Undiagnosed Prediabetes/Type 2 Diabetes, Prehypertension/Hypertension and Obesity Among Ethnic Groups of Adolescents in Western Canada," *BMC Pediatrics*, vol. 20, no. 1, pp. 1-9, 2020. *Crossref*, https://doi.org/10.1186/s12887-020-1924-6

[4] Raphael D. Ayivi et al., "Lactic Acid Bacteria: Food Safety and Human Health Applications," *Dairy*, vol. 1, no. 3, pp. 202-232, 2020. *Crossref*, https://doi.org/10.3390/dairy1030015

[5] Irini Chatziralli, "Ranibizumab for the Treatment of Diabetic Retinopathy," *Expert Opinion on Biological Therapy*, vol. 21, no. 8, pp. 991-997, 2021. *Crossref*, https://doi.org/10.1080/14712598.2021.1928629

[6] Prawej Ansari et al., "Diabetic Retinopathy: An Overview on Mechanisms, Pathophysiology and Pharmacotherapy," *Diabetology*, vol. 3, no. 1, pp. 159-175, 2022. *Crossref*, https://doi.org/10.3390/diabetology3010011

[7] N. Durga, Dr. D. Kerana Hanirex, and Dr. A. Muthukumaravel, "A Systematic Review on Diabetic Retinopathy and Common Eye Diseases Detection through Deep Learning Techniques," *Journal of Positive School Psychology*, vol. 6, no. 4, pp. 1905-1919, 2022.

[8] Stela Vujosevic et al., "Screening for Diabetic Retinopathy: New Perspectives and Challenges," *The Lancet Diabetes & Endocrinology*, vol. 8, no. 4, pp. 337-347, 2020. *Crossref*, https://doi.org/10.1016/S2213-8587(19)30411-5

[9] Karthik Kumar et al., "Clinical Features and Surgical Outcomes of Complications of Proliferative Diabetic Retinopathy in Young Adults with Type 1 Diabetes Mellitus Versus Type 2 Diabetes Mellitus-A Comparative Observational Study," *Indian Journal of Ophthalmology*, vol. 69, no. 11, pp. 3289-3295, 2021. *Crossref*, https://doi.org/10.4103/ijo.IJO_1293_21

[10] Daniel Yim et al., "Barriers in Establishing Systematic Diabetic Retinopathy Screening through Telemedicine in Low-and Middle-Income Countries," *Indian Journal of Ophthalmology*, vol. 69, no. 11, pp. 2987-2992, 2021. *Crossref*, https://doi.org/10.4103/ijo.IJO_1411_21

[11] Charles C Wykoff et al., "Risk of Blindness Among Patients with Diabetes and Newly Diagnosed Diabetic Retinopathy," *Diabetes Care*, vol. 44, no. 3, pp. 748-756, 2021. *Crossref*, https://doi.org/10.2337/dc20-0413

[12] Emma Beede et al., "A Human-Centered Evaluation of a Deep Learning System Deployed in Clinics for the Detection of Diabetic Retinopathy," *Proceedings of the 2020 CHI Conference on Human Factors in Computing Systems*, pp. 1-12. 2020. *Crossref*, https://doi.org/10.1145/3313831.3376718

[13] Ursula Schmidt-Erfurth et al., "AI-Based Monitoring of Retinal Fluid in Disease Activity and Under Therapy," *Progress in Retinal and Eye Research*, vol. 86, p. 100972, 2022. *Crossref*, https://doi.org/10.1016/j.preteyeres.2021.100972

[14] Christian Enders et al., "Comparison Between Findings in Optical Coherence Tomography Angiography and in Fluorescein Angiography in Patients with Diabetic Retinopathy," *Ophthalmologica*, vol. 243, no. 1, pp. 21-26, 2020. *Crossref*, https://doi.org/10.1159/000499114

[15] Md Mohaimenul Islam et al., "Deep Learning Algorithms for Detection of Diabetic Retinopathy in Retinal Fundus Photographs: A Systematic Review and Meta-Analysis," *Computer Methods and Programs in Biomedicine*, vol. 191, p. 105320, 2020. *Crossref*, https://doi.org/10.1016/j.cmpb.2020.105320

[16] Isabella Castiglioni et al., "AI Applications to Medical Images: From Machine Learning to Deep Learning," *Physica Medica*, vol. 83, pp. 9-24, 2021. *Crossref*, https://doi.org/10.1016/j.ejmp.2021.02.006

[17] Julia Amann et al., "Explainability for Artificial Intelligence in Healthcare: A Multidisciplinary Perspective," *BMC Medical Informatics and Decision Making*, vol. 20, no. 1, pp. 1-9, 2020. *Crossref*, https://doi.org/10.1186/s12911-020-01332-6

[18] Sujata Chaudhari et al., "Yolo Real Time Object Detection," *International Journal of Computer Trends and Technology*, vol. 68, no. 6, pp. 70-76, 2020. *Crossref*, https://doi.org/10.14445/22312803/IJCTT-V68I6P112

[19] Imran Qureshi, Jun Ma, and Qaisar Abbas, "Diabetic Retinopathy Detection and Stage Classification in Eye Fundus Images Using Active Deep Learning," *Multimedia Tools and Applications*, vol. 80, no. 8, pp. 11691-11721, 2021. *Crossref*, https://doi.org/10.1007/s11042-020-10238-4

[20] V Desika Vinayaki, and R Kalaiselvi, "Multithreshold Image Segmentation Technique using Remora Optimization Algorithm for Diabetic Retinopathy Detection from Fundus Images," *Neural Processing Letters*, vol. 54, no. 3, pp. 2363-2384, 2022. *Crossref*, https://doi.org/10.1007/s11063-021-10734-0

[21] J. Granty Regina Elwin et al., "Ar-HGSO: Autoregressive-Henry Gas Sailfish Optimization Enabled Deep Learning Model for Diabetic Retinopathy Detection and Severity Level Classification," *Biomedical Signal Processing and Control*, vol. 77, p. 103712, 2022. *Crossref*, https://doi.org/10.1016/j.bspc.2022.103712

[22] S.Supraja, and P.Ranjith Kumar, "An Intelligent Traffic Signal Detection System Using Deep Learning," *SSRG International Journal of VLSI & Signal Processing*, vol. 8, no. 1, pp. 5-9, 2021. *Crossref*, https://doi.org/10.14445/23942584/IJVSP-V8I1P102

[23] Eman Abdel Maksoud, Sherif Barakat, and Mohammed Elmogy, "A Computer-Aided Diagnosis System for Detecting Various Diabetic Retinopathy Grades Based on a Hybrid Deep Learning Technique," *Medical & Biological Engineering & Computing*, pp. 2015–2038, 2022. *Crossref*, https://doi.org/10.1007/s11517-022-02564-6

[24] Salisu Ibrahim et al., "Diabetic Retinopathy Detection using Local Extrema Quantized Haralick Features with Long Short-Term Memory Network," *International Journal of Biomedical Imaging*, vol. 2021, 2021. *Crossref*, https://doi.org/10.1155/2021/6618666

[25] Lakshmana Kumar Ramasamy et al., "Detection of Diabetic Retinopathy using a Fusion of Textural and Ridgelet Features of Retinal Images and Sequential Minimal Optimization Classifier," *PeerJ Computer Science*, vol. 7, p. e456, 2021. *Crossref*, https://doi.org/10.7717/peerj-cs.456

[26] Muhammad Kashif Yaqoob et al., "Resnet Based Deep Features and Random Forest Classifier for Diabetic Retinopathy Detection," *Sensors*, vol. 21, no. 11, p. 3883, 2021. *Crossref*, https://doi.org/10.3390/s21113883

[27] Hemavathi S, and Dr.S. Padmapriya, "Detection of Diabetic Retinopathy on Retinal Images using Support Vector Machine," *SSRG International Journal of Computer Science and Engineering – Special Issue ICMR*, pp. 5-8, 2019.

[28] Dr. Shubhangi D C, and Tasleem Begum, "Diagnosis of Diabetic Retinopathy Using Dimensional Reduction Algorithm," *International Journal of Engineering Trends and Technology*, pp. 178-181, vol. 67, no. 10, pp. 178-181, 2019. *Crossref*, https://doi.org/10.14445/22315381/IJETT-V67I10P228

[29] S. Regina Lourdhu Suganthi, U K Sneha, and Shwetha S, "Diabetic Retinopathy Classification Using Machine Learning Techniques," *International Journal of Engineering Trends and Technology*, vol. 68, no. 1, pp. 51-56, 2020. *Crossref*, https://doi.org/10.14445/22315381/IJETT-V68I1P207

[30] Manojkumar S. B, and Sheshadri H. S, "Analysis of Detection of Diabetic Retinopathy using LPB and Deep Learning Techniques," *International Journal of Engineering Trends and Technology*, vol. 68, no. 12, pp. 123-131, 2020. *Crossref*, https://doi.org/10.14445/22315381/IJETT-V68I12P221

[31] Yue Miao, and Siyuan Tang, "Classification of Diabetic Retinopathy Based on Multiscale Hybrid Attention Mechanism and Residual Algorithm," *Wireless Communications and Mobile Computing*, vol. 2022, 2022. *Crossref*, https://doi.org/10.1155/2022/5441366

[32] Santiago Toledo-Cortés et al., "Grading Diabetic Retinopathy and Prostate Cancer Diagnostic Images with Deep Quantum Ordinal Regression," *Computers in Biology and Medicine*, vol. 145, p. 105472, 2022. *Crossref*, https://doi.org/10.1016/j.compbiomed.2022.105472

[33] Ambaji S. Jadhav, Pushpa B. Patil, and Sunil Biradar, "Optimal Feature Selection-Based Diabetic Retinopathy Detection Using Improved Rider Optimization Algorithm Enabled with Deep Learning," *Evolutionary Intelligence*, vol. 14, no. 4, pp. 1431-1448, 2021. *Crossref*, https://doi.org/10.1007/s12065-020-00400-0

[34] Feng Li et al., "Deep Learning-Based Automated Detection for Diabetic Retinopathy and Diabetic Macular Oedema in Retinal Fundus Photographs," *Eye*, vol. 36, no. 7, pp. 1433-1441, 2022. *Crossref*, https://doi.org/10.1038/s41433-021-01552-8

[35] Muhammad Mohsin Butt et al., "Diabetic Retinopathy Detection from Fundus Images of the Eye Using Hybrid Deep Learning Features," *Diagnostics*, vol. 12, no. 7, p. 1607, 2022. *Crossref*, https://doi.org/10.3390/diagnostics12071607